Peer reviewed version

Link to published version (if available):
10.1038/s41550-019-0721-3

Link to publication record in Explore Bristol Research
PDF-document

University of Bristol - Explore Bristol Research
General rights

The global geophysical environment of (101955) Bennu

D.J. Scheeres[1], J.W. McMahon[1], A.S. French[1], D.N. Brack[1], S.R. Chesley[2], D. Farnocchia[2], Y. Takahashi[2], J. Leonard[3], J. Geeraert[3], B. Page[3], P. Antreasian[3], K. Getzandanner[4], D. Rowlands[4], E. Mazarico[4], J. Small[4], M. Moreau[4], J. Emery[5], B. Rozitis[6], M. Hirabayashi[7], P. Sanchez[8], S. Van wal[9], P. Tricarico[10], R.-L. Ballouz[11], C.L. Johnson[12], M.M. Al Asad[12], H.C.M. Susorney[12], O.S. Barnouin[13], M.G. Daly[14], R.W. Gaskell[10], E.E. Palmer[10], J.R. Weirich[10], K.J. Walsh[15], E.R. Jawin[16], E.B. Bierhaus[17], P. Michel[18], W.F. Bottke[15], M.C. Nolan[11], D.S. Lauretta[11], H.C. Connolly Jr.[19] and the OSIRIS-REx Team.

[1]Smead Department of Aerospace Engineering, University of Colorado, Boulder, Colorado USA. (scheeres@colorado.edu)
[2]Solar System Dynamics Group, Jet Propulsion Laboratory, Pasadena, California, USA.
[3]KinetX Aerospace, Inc., Simi Valley, CA, USA.
[4]NASA Goddard Space Flight Center, Greenbelt, MD, USA.
[5]University of Tennessee, Knoxville, Tenessee, USA.
[6]Planetary and Space Sciences, School of Physical Sciences, The Open University, Milton Keynes, UK.
[7]Auburn University, Auburn, AL 36849, USA.
[8]Colorado Center for Astrodynamics Research, University of Colorado, Boulder, Colorado USA.
[9]Institute of Space and Astronautical Science (ISAS), Japan Aerospace Exploration Agency (JAXA), Sagamihara 252-5210, Japan.
[10]Planetary Science Institute, Tucson, AZ 85710, USA.
[11]Lunar Planetary Laboratory, University of Arizona, Tucson, AZ, USA.
[12]Department of Earth, Ocean and Atmospheric Sciences, University of British Columbia, Vancouver, Canada.
[13]The Johns Hopkins University Applied Physics Laboratory, Laurel, MD, USA.
[14]The Centre for Research in Earth and Space Science, York University, Toronto, Ontario, Canada.
[15]Southwest Research Institute, Boulder, CO, USA.
[16]Smithsonian Institution National Museum of Natural History, Washington, DC, USA.
[17]Lockheed Martin Space Systems Company, Denver, CO, USA.
[18]Université Côte d'Azur, Observatoire de la Côte d'Azur, CNRS, Laboratoire Lagrange, Nice, France.
[19]School of Earth and Environment, Rowan University, Glassboro, New Jersey, USA.

Global insights into asteroid (101955) Bennu and strong constraints on its dynamical state are documented by combining the asteroid's mass, as measured by the Origins, Spectral Interpretation, Resource Identification, and Security–Regolith Explorer (OSIRIS-REx) mission, with Bennu's shape and spin state. Here we show that analysis of Bennu's geophysical environment presents evidence of a changing surface structure driven by Bennu's changing spin period. Bennu's global shape is consistent with spin-induced failure at some point in its past, although the manner of its failure cannot be determined yet. There is also evidence for significant density heterogeneity within the body. Future results from the OSIRIS-REx mission are expected to resolve questions of its shape formation and evolution.

During the Preliminary Survey phase of the mission (between 3 and 19 December 2018), the OSIRIS-REx spacecraft performed five slow, hyperbolic flybys of Bennu, with closest approach distances of

~7 km and speeds of ~4 cm/s. The spacecraft was tracked using the Deep Space Network to acquire Doppler shift data which, combined with optical navigation images, could detect the small deflection of the spacecraft trajectory due to the asteroid's gravity, which was on the order of 3.5 cm/s [1,2] (methods). These measurements yield a gravitational parameter of 4.892±0.002 m3/s2 (mass of 7.329±0.003 X 10^{10} kg). When combined with the volume of 6.16±0.07 X 10^7 m3 determined from the shape [3], we determine a bulk density of 1190±13 kg/m3. This is consistent with that of asteroid (162173) Ryugu which was measured to be 1190±30 kg/m3 by the Hayabusa2 spacecraft [4]. Using an analog CM chondrite, this yields a macroporosity of 40 to 50% [4], providing additional evidence that Bennu is a rubble-pile asteroid.

Our density estimate is consistent with the previous estimate of 1260±70 kg/m^3 [5], which was based on a detection of the Yarkovsky effect using radar and infrared astronomy rather than gravitational perturbations. We have updated that analysis using the new shape model [3], thermal inertia values [6] and an updated estimate of the Bennu ephemeris. The ephemeris update includes spacecraft observations and refines the semimajor axis drift rate to -19.020 +/- 0.087 x 10^{-4} au/Myr, which is negligibly different from [5]. Applying the same model to fit the Yarkovsky drift rate using these in situ measurements predicts a gravitational parameter of 4.9 ± 0.1 m^3/s^2 which agrees remarkably well with the direct measurements. These results prove that combining remote measurements of shape, semi-major axis drift and thermal inertia is a valid technique for determining masses of asteroids.

Bennu's Geophysical Environment: Using a constant density hypothesis, we evaluate the geophysical environment of Bennu, mirroring and refining the analysis made using pre-encounter models [7]. The geopotential measures relative potential energy across the surface while its gradient yields the acceleration at any given location in a frame rotating with Bennu, including off of its surface. The maximum surface acceleration is 80 μm/s^2 at the poles and smoothly decreases across the surface to the equator, where it reaches a minimum of 26 μm/s^2 (Supplementary Fig. 1). Thus, material across the entire body exists in a microgravity environment, a state of matter that is poorly understood, and where weak cohesive forces compete with gravitational and friction forces [8]. At the equator, a 1-m-radius boulder exerts a pressure of ~0.1 Pa on the surface, and thus a cohesion level of this amount would stabilize a boulder.

The Bennu geopotential is highest at the poles and lowest at the equator, meaning that all of the surface slopes are generally directed toward the equatorial region [9] (Supplementary Fig. 2). Local deviations from this trend occur across the surface and appear to drive the local downslope motion of regolith [10]. A particle rolling downslope from either pole to the equator would acquire, at most, just over 11 cm/s of speed if no energy was lost (Supplementary Fig. 3). At the equator, the minimum speed necessary for a particle to leave the surface ranges from 2 to 4 cm/s, considering the local surface curvature and acceleration [11]. Thus, material can achieve orbit through downslope migration, necessitating a study of dynamics close to the surface.

In the Bennu fixed frame are eight equilibrium points where the gravitational attraction and centripetal acceleration are balanced, resulting in synchronous orbits that remain fixed in the rotating frame [7]. The number of equilibrium points is consistent with the strong degree 4 sectoral coefficients of the shape [3]. For the current model, seven of these equilibria are unstable, and one

is stable (Fig. 1). The presence of the unstable equilibrium points in proximity to the surface creates a chaotic orbital environment for any material lifted from the surface at low speeds.

The geopotential also defines Bennu's rotational Roche lobe, defined as the spatial surface where the geopotential has the same value as the equilibrium point with minimum energy [7]. The lobe is thus the minimum-energy surface that separates Bennu from space, and for Bennu intersects its shape at average latitudes of −22.4° and 23.4°. The region between these latitudes lies within the lobe, while the true intersection point wanders by a few degrees in latitude (Fig. 2). Within this latitude band, any particles lofted with an energy less than the rotational Roche lobe energy, which corresponds to speeds ≤ 4 cm/s, are trapped within the lobe and cannot escape from Bennu and will eventually reimpact the surface between these latitudes (Supplementary Fig. 4). Conversely, speeds that place a particle directly on an escape trajectory range from over 20 cm/s in the polar regions down to 10 cm/s in the equatorial region, and are highly dependent on surface orientation (Supplementary Fig. 4). Between these speeds the outcome can be either reimpact, escape or capture into a longer term stable orbit.

Surface slopes on Bennu are highly sensitive to the resolution of the shape model. However, the overall structure of the slope distributions on Bennu are seen to have the same basic pattern independent of shape resolution. For the 3-m resolution shape model the globally averaged slopes are 15.4°. The latitudes within the rotational Roche lobe have an average slope of 11.8°, whereas the regions outside of the lobe have an average slope of 17.9° in the south (−Z) and 18.8° in the north (+Z) (Fig. 2). The transition in slope closely corresponds to the lobe's intersection with the surface, with the surface within the lobe being more energetically relaxed than the surface outside of the lobe. The dynamics associated with the rotational Roche lobe may have contributed to this. For example, if there were a large cloud of particles orbiting about the Bennu equator, some fraction of those would be trapped within the lobe and would redistribute themselves in this region, whereas those with greater energy or outside of the lobe would preferentially escape. Also, particles that migrate downslope from the higher latitudes (where they otherwise have sufficient energy to escape) become trapped on the surface once they enter this region.

This current observation is the first precise indication that the energetic trapping defined by the rotational Roche lobe may play a role in controlling the shape and topography of the surface, which is important as all fast-spinning, top-shaped asteroids will have similar intersections of their rotational Roche lobes in their mid-latitudes. The latitudes of the lobe intersection are tied to the current spin rate of the asteroid, with a slower rotation rate in the past leading to the lobe having higher-latitude intersections. This indicates that the surface relaxation process may be occurring concurrently with the measured spin rate acceleration described in [12] and consistent with a doubling of Bennu's spin rate in 2 Myr. If the observed increase in rotation rate persisted linearly back in time, 600,000 years ago the asteroid was spinning at a 5-hour period, putting the lobe intersection at ±49°, whereas 1 million years ago the asteroid was spinning at a 8.6-hour period, putting the entire surface within the lobe.

Constraints on the origin of Bennu's shape: Several formation mechanisms have been proposed for spinning top–shaped asteroids, and the OSIRIS-REx mission provides an opportunity to probe and test these theories. A direct interpretation of the surface age of Bennu from crater density indicates

an age of 100 million to 1 billion years [10]. Thus, it is possible that the asteroid's distinctive shape was formed either during accretion [13,14] or during a reshaping event early in its history. However, a primordial shape is inconsistent with the current slope transition at the lobe intersection and the measured acceleration in its rotation period, which suggests that Bennu's surface changes in conjunction with its rotation rate.

An early or initial shape formation would imply that Bennu has avoided going through multiple YORP cycles, periods of more rapid rotation due to small torques arising from asymmetries in its shape, which then lead shape deformations and periods of slower rotation, with the sequence occurring repetitively every few YORP timescales [15,16]. This could be explained if Bennu was trapped in a YORP equilibrium for an extended period of time in the main belt, which would result in no change in its rotation state and hence shape [17]. Under this scenario, the asteroid may have been disturbed only recently from this equilibrium, perhaps by its passage into the inner Solar System [16]. Alternately, it could imply that our understanding of how rubble pile bodies respond to periods of rapid rotation is incomplete.

To study the implications of past spin rates on Bennu's shape, we performed a stress analysis [18]. Figure 3 shows the minimum cohesive strength needed to keep the body from undergoing plastic deformation and the regions where it would first fail at different spin rates. At its current spin period and up to 3.7 hours, a cohesive strength on the order of 0.1 Pa or more is needed to stabilize the surface against landslides. At spin periods of 3.6 hours and faster, a strength of 1 Pa or more is needed to stabilize the interior. A complementary analysis of surface slopes (Fig. 3) shows that at spin periods higher than 3.6 hours, over half of Bennu's surface is at or exceeds an angle of repose of 30° and would definitely fail via landsliding if it were a cohesionless regolith.

If Bennu acquired its distinctive shape after its initial formation, three main mechanisms have been proposed [7]. These are formation by downslope migration of material from mid-latitudes to the equatorial region [19, 20, 21, 22, 23]; failure and collapse of the interior of the body, deforming the surface of the asteroid [18,24]; or the tidal disruption of a natural satellite that fell back onto the asteroid surface [25,26]. The conformity of the slope change with the Roche lobe would be consistent with the infall scenario, as such an event would distribute a large amount of material across the equator at low speeds, which would preferentially settle within the lobe. This scenario seems inconsistent with the age of the surface and the current acceleration of the spin rate, however.

An interior failure could have occurred in the past, and granular mechanics simulations show that if the interior bulged outwards, surface structures could have been maintained without deformation (methods), implying that even a more recent failure mode such as this could be feasible and consistent with an old surface. This failure mode would predict a less dense interior, which would be consistent with gravity coefficients that are larger than the shape-based constant density gravity coefficients.

If, instead, the body has a stronger interior, then the mantle of surface material would fail at a fast spin rate [22]. Comparison of the surface slope distribution at past spin rates shows that the current surface is consistent with failure at a spin rate of 3.6 hours (Fig. 3) and yields a shape that is

consistent with this failure mode (Fig. 4) [20,23]. These findings support the possibility of a denser core, with corresponding lower values of gravity coefficients.

Density Heterogeneity in Bennu: These hypotheses show the importance of constraining the internal density distribution of Bennu. Some initial results along this topic can be extracted from analysis of Bennu's shape, which is constructed such that its origin is at the center of mass and that it spins about its maximum moment of inertia. Under a constant density assumption, the offset between the center of figure and center of mass is [1.4, -0.5, -0.15] m in the Bennu-fixed frame and the products of inertia are $I_{zx} = -46.70$ m^2 and $I_{zy} = 11.39$ m^2 as compared to $I_{zz} = 26{,}780$ m^2 [3]. These measurements correspond to a ~0.1% shift in the center of mass and a ~0.1° offset of the principal axis from a constant density shape and indicate heterogeneity in the mass distribution. To account for this heterogeneity with a minimal model consistent with surface observations and Bennu's rubble pile structure, we assume that Bennu contains two spherical boulders with a particle density twice the measured bulk density (assuming a 50% porosity) and diameters of 80 m (less than the largest boulder outcrop size seen on Bennu [6,10]). These objects would constitute almost 1% of the total mass and would have a density of 2360 kg/m^3 with the bulk density of the remaining body at 1180 kg/m^3. To match the observed asymmetry, both boulders must be displaced in the –x direction, with one of them having its largest extent at the surface, and with both bodies displaced in opposite directions about the equatorial plane with a total separation between them of 200 m (methods, Supplemental Fig. 5). Although this solution is not unique, it establishes that the offsets can be explained in a plausible model.

Future low orbits about Bennu will refine our understanding of the surface and enable us to estimate higher-order gravity field coefficients. This will increase the resolution at which we can detect and constrain Bennu's internal heterogeneities and will provide direct evidence of how the mass is distributed within the body. This, in turn, will enable us to evaluate the competing theories for how its shape formed, or may suggest new alternative models that must be considered.

References
[1] J.W. McMahon, D.J. Scheeres, S.G. Hesar, D. Farnocchia, S. Chesley and D. Lauretta. 2018. "The OSIRIS-REx Radio Science Experiment at Bennu," Space Science Reviews 214:43. https://doi.org/10.1007/s11214-018-0480-y

[2] Williams, B., Antreasian, P., Carranza, E., Jackman, C., Leonard, J., Nelson, D., Page, B., Stanbridge, D., Wibben, D., Williams, K. and Moreau, M., 2018. OSIRIS-REx flight dynamics and navigation design. Space Science Reviews, 214(4), p.69. https://doi.org/10.1007/s11214-018-0501-x

[3] Barnouin O. S. et al. this issue

[4] S. Watanabe, M. Hirabayashi, N. Hirata, N. Hirata, R. Noguchi, Y. Shimaki, H. Ikeda, E. Tatsumi, M. Yoshikawa, S. Kikuchi, H. Yabuta, T. Nakamura, S. Tachibana, Y. Ishihara, T. Morota, K. Kitazato, N. Sakatani, K. Matsumoto, K. Wada, H. Senshu, C. Honda, T. Michikami, H. Takeuchi, T. Kouyama, R. Honda, S. Kameda, T. Fuse, H. Miyamoto , G. Komatsu, S. Sugita, T. Okada, N. Namiki, M. Arakawa,

M. Ishiguro, M. Abe, R. Gaskell, E. Palmer, O. S. Barnouin, P. Michel, A. French, J. W. McMahon, D. J. Scheeres, P. A. Abell, Y. Yamamoto, S. Tanaka, K. Shirai, M. Matsuoka, M. Yamada, Y. Yokota, H. Suzuki, K. Yoshioka, Y. Cho, S. Tanaka, N. Nishikawa, T. Sugiyama, H. Kikuchi, R. Hemmi, T. Yamaguchi, N. Ogawa, G. Ono, Y. Mimasu, K. Yoshikawa, T. Takahashi, Y. Takei, A. Fujii, C. Hirose, T. Iwata, M. Hayakawa, S. Hosoda, O. Mori, H. Sawada, T. Shimada, S. Soldini, H. Yano, R. Tsukizaki, M. Ozaki, Y. Iijima, K. Ogawa, M. Fujimoto, T.-M. Ho, A. Moussi, R. Jaumann, J.-P. Bibring, C. Krause, F. Terui, T. Saiki, S. Nakazawa, Y. Tsuda. 2019. Hayabusa2 observations of the top-shaped carbonaceous asteroid 162173 Ryugu. Submitted to Science.

[5] Chesley, S.R., Farnocchia, D., Nolan, M.C., et al., 2014. Orbit and bulk density of the OSIRIS-REx target asteroid (101955) Bennu. Icarus 235, 5–22.

[6] DellaGiustina et al. This issue

[7] D.J. Scheeres, S. Hesar, S. Tardivel, M. Hirabayashi, D. Farnocchia, J. McMahon, S. Chesley, O. Barnouin, R.P. Binzel, W.F. Bottke, M.G. Daly, J. Emery, C. Hergenrother, D.S. Lauretta, J. Marshall, P. Michel, M. Nolan, and K.J. Walsh. 2016. "The Geophysical Environment of Bennu," Icarus 276: 116-140.

[8] D.J. Scheeres, C.M. Hartzell, P. S`anchez, M. Swift. 2010. "Scaling forces to asteroid surfaces: The role of cohesion," Icarus 210: 968-984.

[9] Lauretta D. S. et al. this issue

[10] Walsh K. J. et al. this issue

[11] S. Van wal and D.J. Scheeres. 2016. "The Lift-Off Velocity on the Surface of an Arbitrary Body," Celestial Mechanics and Dynamical Astronomy 125(1): 1-31.

[12] Hergenrother et al., this issue

[13] Sanchez, D.P. and Scheeres, D.J. 2018. The Role of Angular Momentum on Accreting Rubble Pile Shapes. 49th LPSC, Abstract 1196.

[14] Michel, P., O.S. Barnouin, R.-L. Ballouz, K.J. Walsh, D.C. Richardson, S.R. Schwartz, M. Jutzi, S. Sugita, S. Watanabe, M. Hirabayashi, H. Miyamoto, H.C. Connolly Jr., D.S. Lauretta. 2018, Disruption and Reaccumulation as the Origin of the Ryugu and Bennu Top Shapes? AGU Fall Meeting 2018 abstract P33C-3850.

[15] Statler, T.S., 2009. Extreme sensitivity of the YORP effect to small-scale topography. Icarus 202, 502–513.

[16] W.F. Bottke, D. Vokrouhlický, K.J. Walsh, M. Delbo, P. Michel, D.S. Lauretta, H. Campins, H.C. Connolly Jr., D.J. Scheeres, S.R. Chelsey. 2015. "In search of the source of asteroid (101955) Bennu: Applications of the stochastic YORP model," Icarus 247: 191-217.

[17] O. Golubov and D.J. Scheeres. "Systematic structure and sinks in the YORP effect," Astrophysical Journal, in press, 1/2019.

[18] Hirabayashi, M., Scheeres, D.J., 2015. Stress and failure analysis of rapidly rotating asteroid (29075) 1950 DA. Astrophys. J. Lett. 798 (1), L8.

[19] Minton, D.A., 2008. The topographic limits of gravitationally bound, rotating sand piles. Icarus 195 (2), 698–704.

[20] Harris, A.W., Fahnestock, E.G., Pravec, P., 2009. On the shapes and spins of 'rubble pile' asteroids. Icarus 199 (2), 310–318.

[21] Walsh, K.J., Richardson, D.C., Michel, P., 2012. Spin-up of rubble-pile asteroids: disruption, satellite formation, and equilibrium shapes. Icarus 220 (2), 514–529.

[22] Hirabayashi, M., Sánchez, P., Scheeres, D.J., 2015. Internal structure of asteroids having surface shedding due to rotational instability. Astrophys. J. 808 (1), 63.

[23] D.J. Scheeres. 2015. "Landslides and Mass Shedding on Spinning Spheroidal Asteroids," Icarus 247: 1-17.

[24] M. Hirabayashi and D.J. Scheeres. 2019. "Rotationally induced failure of irregularly shaped asteroids," Icarus 317: 354-364.

[25] D. J. Scheeres, E. G. Fahnestock, S. J. Ostro, J.-L. Margot, L. A. M. Benner, S. B. Broschart, J. Bellerose, J. D. Giorgini, M. C. Nolan, C. Magri, P. Pravec, P. Scheirich, R. Rose, R. F. Jurgens, S. Suzuki, E. M. DeJong. 2006. "Dynamical Configuration of Binary Near-Earth Asteroid (66391) 1999 KW4," Science 314: 1280-1283.

[26] S.A. Jacobson and D.J. Scheeres. 2011. "Dynamics of Rotationally Fissioned Asteroids: Source of Observed Small Asteroid Systems," Icarus 214(1): 161-178.

Corresponding Author
Daniel J. Scheeres (scheeres@colorado.edu)

Author contributions
DJS led the analysis and writing of the paper; JWM led the University of Colorado (CU) estimation activities; ASF performed the estimation for CU; DNB supported tasks at CU; SRC led the Yarkovsky and ephemeris update team at JPL; DF and YT performed the ephemeris estimation at JPL; JL lead

the orbit determination activity at KinetX, supported by JG and BP; PA led the navigation team for OSIRIS-REx; KG led the estimation activities at GSFC and was supported by DR, EM and JS; MM led the joint Flight Dynamics team; JE and BR analyzed the thermal data for the Yarkovsky density estimate; MH performed the Bennu stress analysis; PS performed granular mechanics simulations; SVW analyzed speed limits on the Bennu surface; PT supported the analysis of density heterogeneities; RLB provided analysis of the surface; CLJ, MMAA and HCMS supported interpretation of the estimated shape model; OSB led the shape modeling activity; MGD provided analysis support of the shape model; RWG, EEP, and JRW produced shape models; KJW and ERJ provided interpretation of surface geology; EBB provided interpretation of surface cratering; PM and WFB provided analysis support; MCN, DSL and HCC provided analysis support and scientific leadership; the entire OSIRIS-REx team made this mission possible.

Author information

[1]Smead Department of Aerospace Engineering, University of Colorado, Boulder, Colorado USA. (scheeres@colorado.edu)

[2]Solar System Dynamics Group, Jet Propulsion Laboratory, Pasadena, California, USA.

[3]KinetX Aerospace, Inc., Simi Valley, CA, USA.

[4]NASA Goddard Space Flight Center, Greenbelt, MD, USA.

[5]University of Tennessee, Knoxville, Tenessee, USA.

[6]Planetary and Space Sciences, School of Physical Sciences, The Open University, Milton Keynes, UK.

[7]Auburn University, Auburn, AL 36849, USA.

[8]Colorado Center for Astrodynamics Research, University of Colorado, Boulder, Colorado USA.

[9]Institute of Space and Astronautical Science (ISAS), Japan Aerospace Exploration Agency (JAXA), Sagamihara 252-5210, Japan.

[10]Planetary Science Institute, Tucson, AZ 85710, USA.

[11]Lunar Planetary Laboratory, University of Arizona, Tucson, AZ, USA.

[12]Department of Earth, Ocean and Atmospheric Sciences, University of British Columbia, Vancouver, Canada.

[13]The Johns Hopkins University Applied Physics Laboratory, Laurel, MD, USA.

[14]The Centre for Research in Earth and Space Science, York University, Toronto, Ontario, Canada.

[15]Southwest Research Institute, Boulder, CO, USA.

[16]Smithsonian Institution National Museum of Natural History, Washington, DC, USA.

[17]Lockheed Martin Space Systems Company, Denver, CO, USA.

[18]Université Côte d'Azur, Observatoire de la Côte d'Azur, CNRS, Laboratoire Lagrange, Nice, France.

[19]School of Earth and Environment, Rowan University, Glassboro, New Jersey, USA.
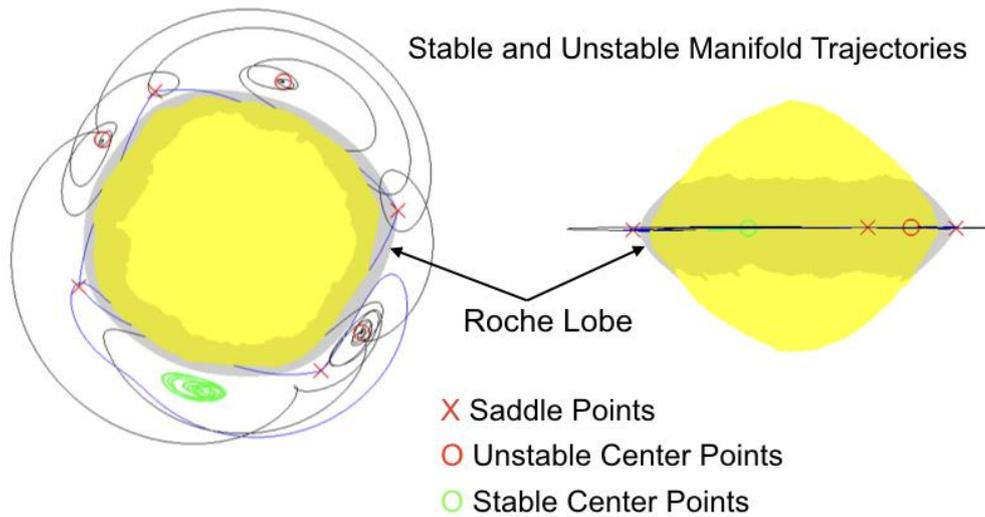
Main figure legends (and figures)

Figure 1: **Equilibrium points in the Bennu-fixed frame, shown with stable and unstable manifolds emanating from the unstable points, and showing a stable trajectory in the vicinity of the stable equilibrium point.** The manifolds control dynamical motion close to Bennu's surface and create a chaotic orbit environment that would redistribute lofted material. The Roche lobe and its intersection with the surface is also shown, emanating from the minimum-energy equilibrium point.
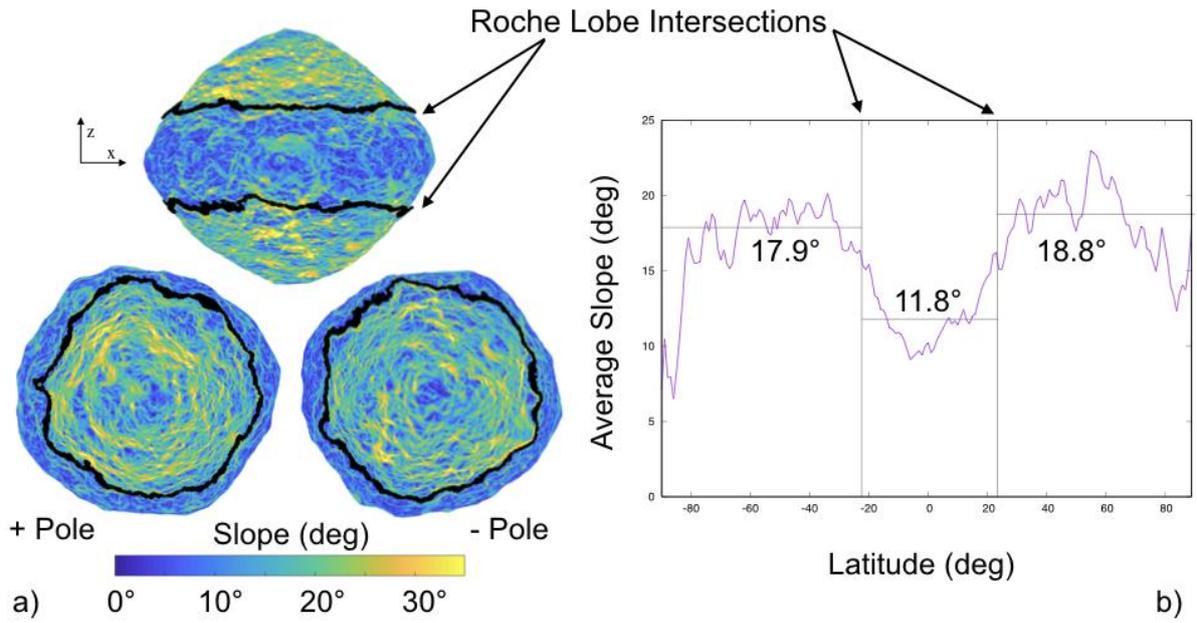
Figure 2: **Surface slope distributions on Bennu in relation to the rotational Roche lobe.** a): Slope distribution for the 3-m Bennu shape model shown with the rotational Roche lobe intersection with the surface. The slope transition is seen to closely follows the lobe intersection region. b): Longitudinally averaged slope as a function of latitude, showing the average slopes within and outside of the lobe. The averaging is over 1-degree-latitude bins.
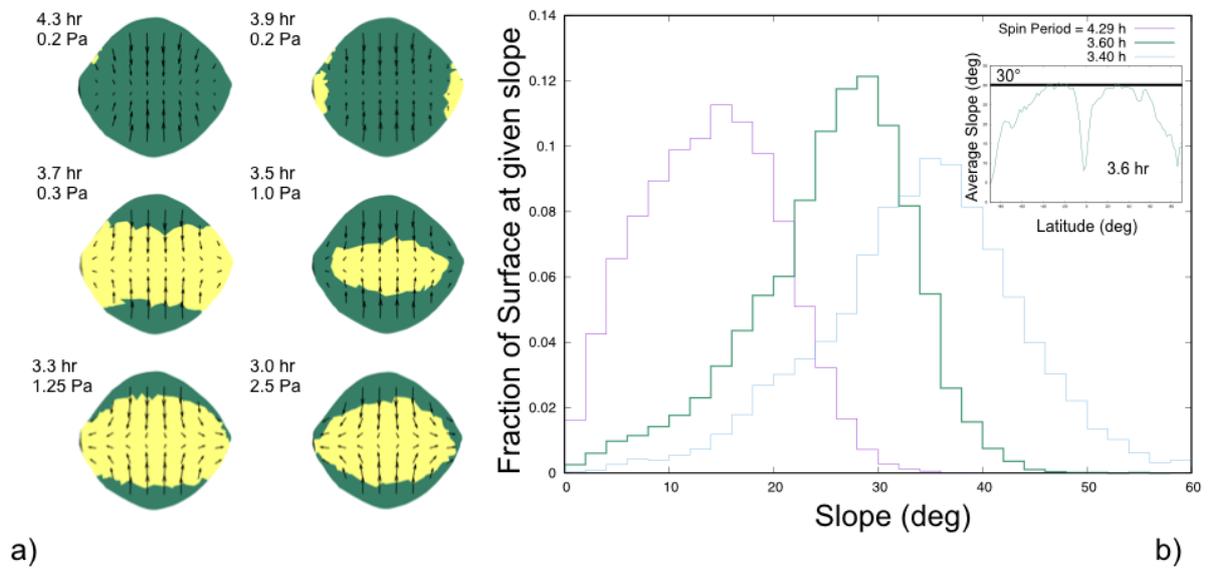
Figure 3: **Failure patterns as a function of Bennu spin rates.** a): Regions of shape stability (green) and plastic deformation (yellow, with arrows showing the direction of failure) at different spin periods and strengths. Under a uniform density and strength distribution assumption, Bennu requires less than 0.3 Pa of strength to retain surface stability up to a spin period of 3.7 hours. At faster spin periods failure occurs across the interior of the body, and requires a strength of at least 1 Pa to maintain the current shape. b): The surface slope distribution has its accumulation point at around 3.6 hours, beyond which the majority of the surface is beyond the usual 30° angle of repose for cohesionless material. The inset shows the average slope as a function of latitude at a 3.6-hour spin period.
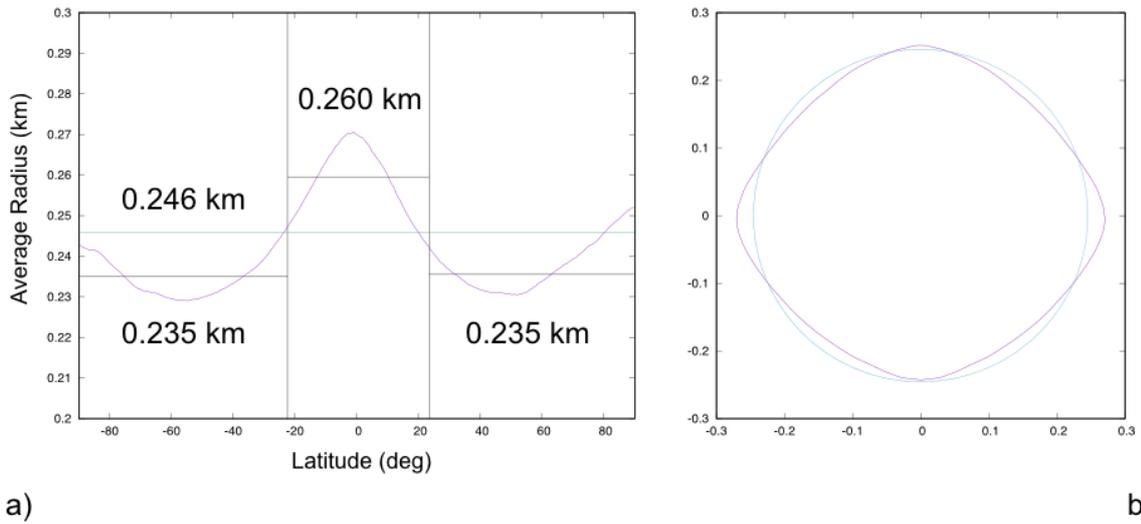
Figure 4: **The longitudinally averaged Bennu radius as a function of latitude (a) and its shape profile compared with its average radius (b).** The smaller radius at mid-latitudes, pole radii close to the mean radius, and exuded equator constitute a predicted profile for a global surface landslide [23].

Methods

Mass Measurement and Estimation:

The Bennu mass measurement experiment carried out by the OSIRIS-REx mission involved several teams each using unique combinations of software tools and data processing techniques. The Radio Science teams were based at the University of Colorado in the Colorado Center for Astrodynamics Research (CU) and at the Jet Propulsion Laboratory in the Solar System Dynamics group (JPL). The navigation and flight dynamics teams were represented by KinetX Corporation with a team in residence at Lockheed Martin's Waterton Campus in Denver (KX) and a team at Goddard Space Flight Center (GSFC). The mass estimates and other fitting data from each team were compared against each other and found to converge to the same mass value within the expected errors. The specific value quoted in the paper is from the CU estimate, however all other estimates agreed to this value within the quoted error estimates as of early January.

The OSIRIS-REx spacecraft began the Approach Phase towards asteroid Bennu on August 17th, 2018. During approach the spacecraft performed six maneuvers to decelerate the spacecraft with respect to Bennu and place it at the Preliminary Survey starting location on December 3rd, 2018. Preliminary Survey consisted of five flybys - three over the north pole, one over the equator, and one over the south pole - and two transition legs. Each flyby started approximately 18.5 km from Bennu, took 48 hours to complete, and achieved a closest approach of 7.5 km at the 24 hour mark. The polar flybys were along the terminator and the equatorial flyby was on the sunlit side. All flyby and transition arcs were joined by maneuvers that varied between 20 and 40 cm/s.

Images taken by spacecraft cameras (POLYCAM, MAPCAM, NAVCAM1) [26] were used to generate center-finding optical navigation data [27]. Optical navigation images were taken between 3 and 7 times per week during approach and every 2 hours during Preliminary Survey. These data, along with X-Band Two-way Doppler, Two-way Range and Delta-Differential One-way Range (Delta-DOR) from the Deep Space Network (DSN), were used to determine both the spacecraft trajectory and Bennu's ephemeris. Mission tracking data will be delivered to the Planetary Data System.

Solution Methods Summaries:

University of Colorado: The CU Radio Science orbit determination solutions were computed using JPL's Mission Analysis, Operations and Navigation Toolkit Environment (MONTE). Two-way Doppler and Two-way Range were weighted per-pass and per antenna at twice their observed noises to prevent over-fitting to imperfectly calibrated data. Per-pass range biases were estimated with an a priori uncertainty of 10 Range Units (RU), where 7.022 RU = 1 meter. DDOR was weighted at 0.06 nanoseconds, the recommended value provided by the DSN. Optical center-finding sample and line were weighted at 0.5 pixels on approach and de-weighted to 2.0 pixels during preliminary survey to account for the increase in Bennu's apparent diameter.

Non-gravitational perturbations to the spacecraft trajectory were characterized prior to the start of Preliminary Survey in order to minimize aliasing between solar pressure, stochastic accelerations, and GM. Area scale factors for each of the sun-ward facing plates were estimated on approach to account for solar pressure and thermal radiation mis-modeling. The plate areas were then held fixed during Preliminary Survey and a single solar pressure scale factor was estimated. Stochastic accelerations were estimated in 12 hour batches with an a priori uncertainty of 5E-13 km/s2. Due to the regular cadence of the flyby/maneuver cycle the stochastic accelerations were correlated exponentially with a 3-day time constant after M1P to prevent interplay with the GM and the maneuvers. In addition to these, parameters estimated in the solution included the spacecraft state

at epoch, the Bennu ephemeris, momentum wheel desaturation maneuvers, targeting maneuver thrust and pointing, per-pass range biases and the Bennu gravitational parameter.

The final reconstructed uncertainty for the spacecraft's Bennu-relative state averaged approximately 5 meters in position and 0.2 mm/s in velocity for each axis, 3-sigma. Solutions were generated for various data weights, stochastic uncertainties/batch lengths/correlation times. It was noted that the GM trended lower with tighter radio weights and/or larger stochastic uncertainty, however all solutions produced both trajectories and GM's consistent to the 1-sigma level.

KinetX: The OSIRIS-REx navigation team's best-estimate of the Bennu GM following the Preliminary Survey phase is 4.89 +/- 0.006 (1-sigma) m^3/s^2.

Extensive work went into modeling the spacecraft down to the acceleration level of $1.0x10^{-13}$ km/s^2 level going into the first North Pole Flyby of Bennu. Throughout cruise, the approach taken by the OSIRIS-REx Orbit Determination team was to model every deterministic acceleration using physics based models. No non-physical scaling of the Solar Radiation Pressure was used. A 10 plate box-wing model was used for the spacecraft with measured areas obtained from pre-launch 3D models. Documentation from Lockheed Martin and closeout photos of the spacecraft in flight configuration were used to determine the material covering of each surface as well as the specular and diffuse reflectivity coefficients. Coordination with the LM thermal team provided a detailed thermal re-radiation model of the spacecraft surfaces for the 10 plate model as well as the addition of the radiators located on the –Z deck of the spacecraft. The model developed with the LM thermal team spanned predicted temperatures for each panel over various solar distances and off sun angles. This approach was taken due to the fact that the passive Lambertian assumption for diffuse radiation of the surfaces did not accurately model the thermal re-radiation effects as seen from an active spacecraft. This thermal re-radiation model along with the estimation of the specular and diffuse re-radiation coefficients of the 10 plate SRP model produced model that matched the pre-launch surface properties and acceleration accuracies to less than 0.5% of the SRP acceleration. This model continuously predicted the approach trajectory to less than 1-sigma of the predicted trajectory uncertainties with random fluctuations in estimated stochastic accelerations on the order of $0.5x10^{-13}$ km/s^2 1-sigma. These additional estimated accelerations were correlated with increased spacecraft activities and off-nominal attitude orientations not seen during cruise.

In addition to the SRP and thermal modeling, the OD team was able to estimate discrepancies between the internal electronic path delays provided pre-launch and what was continuously seen in flight. Coordination with the Telecom team provided corrections to the radiometric data based on the location of the antenna phase-center offsets. All antenna phase-center offsets were estimated in flight during slewing activities to confirm the pre-launch provided locations. All ground station and EOP corrections were updated to coincide with those recommended by the IERS 2010 conventions. Ground station locations are corrected based on solid tides, pole tides, ocean tides, polar motion and continental drift. An acceleration correction due to the electromagnetic radiation pressure of the HGA and LGA antennas as well as OLA was modeled throughout approach.

The OD team estimated the spacecraft state, finite maneuvers, desaturation maneuvers, per-pass range biases, Bennu Ephemeris, stochastic un-modeled accelerations, and SRP scaling. Radiometric data of 2-Way Range and Doppler, DDOR and Optical Images using Gaussian 2D fitting, phase corrections and cross-correlation limb fitting techniques were the primary source of observables processed. Prior to the initial Preliminary North Pole flyby, the navigation team trended the

estimated solution parameters. No stochastic accelerations were estimated after the first Preliminary Survey. This was done to make sure no soak up parameters masked the gravity signal during the flybys.

GSFC: Members of the Flight Dynamics Team located at NASA Goddard Space Flight Center (GSFC) generated an independent spacecraft trajectory solution and Bennu GM estimate at the end of the Preliminary Survey (PS) phase. This solution utilized the GEODYN orbit determination and geophysical parameter estimation software package, also developed and maintained at GSFC [28].

The GSFC solution included DSN radiometric (sequential range, Doppler, and DDOR) and center-finding optical navigation (OpNav) measurement types. The center-finding measurements were constructed by processing MapCam and NavCam images in the Goddard Image Analysis and Navigation Tool (GIANT) [29]. GIANT uses stars in adjoining long exposure images to provide precise absolute (inertial) pointing information interpolated to the epoch of short exposure images containing Bennu's full extent. The center of Bennu in the image is determined precisely through 2D cross-correlation of Bennu's illuminated shape in the image along with a rendered template of the estimated shape model. The model used for PS was constructed by OSIRIS-REx Altimetry Working Group (AltWG) member Dr. Robert Gaskell using Stereophotoclinometry [30] based on Approach PolyCam imagery and delivered on November 27th, 2018. The measurement data weights for DSN Sequential Range were 21 Range Units, for DSN 2-Way Doppler were 5.5 mHz, for DSN Delta-Differenced One-Way Range were 0.06 ns, and for OpNAV Center-finding were 1 pixel. Direct altimetry data from the OSIRIS-REx Laser Altimeter (OLA) [31] taken during four of the PS flybys were processed along with the other measurement data types but not included in the final solution.

The final PS arc started on December 3rd and ended on December 24th. A summary of the estimated parameter list included the spacecraft and asteroid epoch states, the Bennu gravitational parameter, spacecraft maneuvers and momentum wheel desaturations, 3-axis stochastic accelerations with a priori uncertainties of 1 nm/s^2 and per pass range biases with 2 meter apriori uncertainty. Force modeling included point mass gravitation (Sun, 8 Planets + Pluto), Bennu non-spherical gravity (15x15 assuming uniform density), 11-plate solar radiation pressure (SRP), spacecraft thermal radiation, and stochastic accelerations. Temperatures for the thermal radiation model were provided by the spacecraft team at Lockheed Martin as originally requested by KinetX Aerospace. Reconstructed spacecraft attitude and panel orientation information was also provided by the spacecraft team. In addition to the integration and estimation of the OSIRIS-REx trajectory, the orbit of Bennu itself is concurrently integrated and estimated as well. The *a priori* initial state and fully-correlated covariance for Bennu was obtained from the OSIRIS-REx Radioscience Working Group and the JPL Solar System Dynamics Group (Solution #103, Delivered November 8th) [32]. All spacecraft maneuvers (M2P through M1A) were modeled as impulsive V's with *a priori* values and uncertainties provided by the spacecraft team via Maneuver Implementation Files (MIFs). Initial values for spacecraft momentum desaturations were derived from the number of pulse counts provided in the Small Forces File (SFF) and trending data since launch.

Density Heterogeneity Constraint Computations:

To develop a simple yet physically feasible model to fit the non-zero center of mass and product of inertia information with a density distribution we implement the following algorithm and approach.

Density: Assuming a 50% porosity we consider mass contributions to be twice the bulk density. Note, this is equivalent — but opposite — to introducing zero density voids into the body.

Size: The largest body observed on Bennu is at most 80 m in diameter (one dimension). Taking this as a limiting value, we choose boulders of 80 m in diameter. Using a smaller size will require the masses to be pushed farther from the center of the asteroid. This sets the masses of the two boulders and yields the following.
 Mass fractions of the shape and individual grains are 0.9914 and 0.0043, respectively. Bulk densities of the shape and individual grans are 1178 and 2356, respectively.

Constraints:
The center of mass provides three constraints that need to be satisfied by the grain locations, captured in a single vector equation

$$M_0 \mathbf{r}_{COF} + M_1 \mathbf{r}_1 + M_2 \mathbf{r}_2 = 0$$

The products of inertia, assuming mass normalized values, provide two additional equations
$$M_0 I_{xz} - M_1 x_1 z_1 - M_2 x_2 z_2 = 0$$
$$M_0 I_{yz} - M_1 y_1 z_1 - M_2 y_2 z_2 = 0$$

The system as specified is over constrained, with 6 free variables (position vectors of each body) and 5 constraints. To reduce this we introduce an additional constraint, forcing the boulders to have a fixed relative offset in the z-coordinate:

$$z_2 - z_1 - z_1 \Delta Z = 0$$

where ΔZ is a free parameter. If it is greater than -1 the two masses are on the same side of the equator, if -1 then both are zero — meaning that a z component in the center of mass cannot be accommodated, if less than -1 then they are on opposite sides. With this constraint we can then solve for the z-components as
$$z_1 = -\frac{M_0 z_0}{M_1 + M_2 + M_2 \Delta Z}$$

$$z_2 = -\frac{(1 + \Delta Z) M_0 z_0}{M_1 + M_2 + M_2 \Delta Z}$$

and then solve the resulting linear equations for the x-y components to find:

$$x_1 = -\frac{M_0}{M_1 (z_2 - z_1)} \left[I_{xz} - x_0\ z_0 + x_0\ z_2 \right]$$

$$x_2 = \frac{M_0}{M_2(z_2 - z_1)} \left[I_{xz} - x_0\, z_0 + x_0\, z_1 \right]$$

$$y_1 = -\frac{M_0}{M_1(z_2 - z_1)} \left[I_{yz} - y_0\, z_0 + y_0\, z_2 \right]$$

$$y_2 = \frac{M_0}{M_2(z_2 - z_1)} \left[I_{yz} - y_0\, z_0 + y_0\, z_1 \right]$$

Finally, to chose the nominal values we vary the parameter ΔZ over the interval (-1.86, -1.96) to find locations that are nominally within Bennu. The value used in the paper is -1.9, which places the outermost of these points deepest within the body, allowing for their 40 m radius to just lie at the surface. Supplemental Figure 5 shows this plotted on top of the average radius shape model.

Bennu's Geophysical Environment Computations and Supporting Results:

The methods and supporting documentation on how the geophysical environment items were computed is summarized and presented in greater detail in [33]. When applied to the current estimate of the Bennu shape, mass and spin state this yields computations of the surface acceleration, the surface geopotential energy, the return speed, the escape speed and the slopes and slope directions. With the exception of the slope, these computations all appear similar to that reported to the pre-arrival model, albeit with definite values now. Thus, these are presented below with some notes.

Equilibrium Point Computation and Characterization:

The Bennu equilibrium points are computed following the algorithm in [34] and their stability evaluated as described in [33]. Bennu is found to have 8 synchronous orbits close to its surface. Four of these are hyperbolically unstable saddle points, while the other four are center equilibrium points and can either be stable or unstable. For the current model three of these center equilibria are unstable and one is stable, (Fig. 1). The presence of a stable equilibrium point implies that there is a zone about the body where particles, if placed appropriately, can remain in orbit indefinitely about a region in the body-fixed frame. This stable equilibrium point has three distinct oscillation frequencies, two in-plane with periods of 5.8 and 8.6 hours, and one out-of-plane a period of 3.9 hours. The stability of this point is sensitive to the detailed gravity field of the asteroid, and thus may be updated once higher order gravity field coefficients are estimated.

The remaining equilibria are hyperbolically unstable, with characteristic times for the saddle points ranging from 1 to 1.4 hours and 2.6 to 3.4 hours for the unstable center points. All have stable out of plane oscillations with periods around 3.9 hours. The expected presence of heteroclinic tangles associated with these equilibrium points (specifically, associated with manifolds from periodic orbits and quasi-periodic orbits in their vicinity) creates a chaotic orbital environment for any material lifted from the surface at low speeds.

Roche lobe Computation:

The Roche lobe is found by finding the lowest geopotential energy of the eight equilibrium points, which turns out to be the one that lies close to the positive x-axis. Given this Roche lobe energy, we adjust the radii of a chosen shape model until the point reaches this energy value, computed with a relative precision of 10^{-5}. Vertices that are within 1 meter of the surface are considered to be locations where the lobe is intersecting the asteroid surface, and are plotted as black points in Fig. 2. This computation is independent of the slope computations, meaning that transitions seen in the figure are not adjusted in any way, and represent the true variation. To compute the lobe at different spin periods, the entire process is repeated, including finding the new equilibrium points.

Stress and Deformation Analysis of Bennu:

The methodology for computing the stress and failure analysis of Bennu is outlined in [24]. The computations assume a uniform density and strength distribution, and an angle of friction of 35°. The computations were carried out using ANSYS Mechanical APDL (17.0) on the Auburn University Hopper supercomputing system. Additional runs were made that varied the internal density — for both a higher and a lower density — but did not see any substantial deviation in the necessary strengths or spin periods at failure. Future analysis will use more detailed maps of internal density distribution to probe the asteroid failure state due to periods of high rotation.

To probe the effect of an internal deformation on the surface regolith, the granular mechanics model outlined in [35] was applied to a representative longitude lune, starting at a spherical shape and distorting it into an equatorial bulge to mimic the Bennu ridge. For both cohesionless and cohesive grains we did not observe significant distortion of the surface material, consistent with features on the surface potentially being retained during a period of shape deformation due to internal failure.

To analyze the global shape and trends across the surface, the slope and radius of Bennu was averaged over longitude within latitude bands of 1°. To perform these averages all facets with a centroid within a given latitude interval were identified, and the quantity of interest was multiplied by the differential area of the latitude band (computed at the local radius value) and summed, in effect performing an average across the longitude of the asteroid. This quantity was then divided by the summed total area of these regions, performing an area normalized average of the quantity. The averages were performed across the 3 m resolution shape model, which has about 200,000 facets, providing on average over 1000 facets per latitude bin.

Data Availability Statement

Spacecraft tracking data and ancillary files will be available via the Small Bodies Node of the Planetary Data System (https://pds-smallbodies.astro.umd.edu/. Higher-level products, e.g., slope maps, will be available in the Planetary Data System 1 year after departure from the asteroid.

Additional references only in the Methods

[26] B. Rizk, C. Drouet d'Aubigny, D. Golish, C. Fellows, C. Merrill, P. Smith, M. S. Walker, J. E. Hendershot, J. Hancock, S. H. Bailey, D. N. DellaGiustina, D. S. Lauretta, et al. 2018. OCAMS: The OSIRIS-REx Camera Suite, Space Science Reviews 214:26.

[27] Pelgrift, John Y., Eric M. Sahr, Derek S. Nelson, Coralie D. Jackman, Lylia Benhacine, Brent J. Bos, Bashar Rizk et al. "In-flight calibration of the OSIRIS-REx optical navigation imagers." In 1st Annual RPI Workshop on Image-Based Modeling and Navigation for Space Applications. 2018.

[28] Pavlis, D. E., Wimert, J., and McCarthy, J. J., *GEODYN II Systems Description, Vols. 1-5*, 2014. Contract. Rep., SGT Inc., Greenbelt, MD.

[29] Wright, C., Liounis, A., Ashman, B., "Optical Navigation Algorithm Performance," *1st Annual RPI Workshop on Image-Based Modeling and Navigation for Space Applications*, Troy, NY, 2018.

[30] Gaskell, R.W., "Automated Landmark Identification for Spacecraft Navigation," *AAS/AIAA Astrodynamics Specialists Conference* , Quebec City, Canada, 2001. AAS Paper 01-422.

[31] Daly, M., Barnouin, O., et. al., "The OSIRIS-REx Laser Altimeter (OLA) Investigation and Instrument," *Space Science Reviews*, Vol. 212, No. 1-2, 2017, pp. 899-924.

[32] Farnocchia, D., et. al., "Asteroid 101955 Bennu Ephemeris Delivery, JPL Solution 103," JPL IOM 392R-18-005. November 16, 2018.

[33] D.J. Scheeres. "Orbital Motion in Strongly Perturbed Environments: Applications to Asteroid, Comet and Planetary Satellite Orbiters," Springer-Praxis Books in Astronautical Engineering. 2012. ISBN 978-3-642-03255-4

[34] S. Tardivel and D.J. Scheeres "Dynamical structures for the study of irregular grav- ity fields," paper presented at the 2017 AAS/AIAA Space Flight Mechanics Meeting, February 2017. Paper AAS 17-258.

[35] S. Tardivel, P. Sanchez and D.J. Scheeres. 2018. "Equatorial cavities on asteroids, an evidence of fission events," Icarus 304: 192-208.

Figures

See above.